Molecular Cancer

RESEARCH

Open Access

Myofibroblast-derived extracellular vesicles facilitate cancer stemness of hepatocellular carcinoma via transferring ITGA5 to tumor cells

Yang Xiao[1,2†], Ping Tao[3†], Keke Zhang[1†], Liuyan Chen[1], Jinyu Lv[1], Zhiwei Chen[3], Lu He[4], Hongling Jia[5], Jian Sun[3], Mingrong Cao[3], Jian Hong[1,3*] and Chen Qu[1*]

Abstract

Background Myofibroblasts constitute a significant component of the tumor microenvironment (TME) and play a pivotal role in the progression of hepatocellular carcinoma (HCC). Integrin α5 (ITGA5) is a crucial regulator in myofibroblasts of malignant tumors. Therefore, the potential of ITGA5 as a novel target for the therapeutic strategy of HCC should be investigated.

Methods Digital scanning and analysis of the HCC tissue microarray were performed to locate the distribution of ITGA5 and conduct the prognosis analysis. CRISPR Cas9-mediated ITGA5 knockout was performed to establish the ITGA5-KO myofibroblast cell line. Extracellular vesicles (EVs) derived from LX2 were extracted for the treatment of HCC cells. Subsequently, the sphere-forming ability and the stemness markers expression of the treated HCC cells were examined. An orthotopic HCC mouse model with fibrotic injury was constructed to test the outcomes of ITGA5-targeting therapy and its efficacy in the programmed death-ligand 1 (PD-L1) treatment. Co-immunoprecipitation/mass spectrometry and transcriptome data were integrated to delve into the mechanism.

Results The tissue microarray results revealed that ITGA5 was highly enriched in the stromal myofibroblasts of HCC tissues and contributed to enhanced tumor progression and poor prognosis. Notably, ITGA5 transmission via extracellular vesicles (EVs) from myofibroblasts to HCC cells induced the acquisition of cancer stem cell-like properties. Mechanistically, ITGA5 directly bind to YES1, facilitating the activation of YES1 and its downstream pathways, thereby enhancing the stemness of HCC cells. Furthermore, the blockade of ITGA5 impeded tumor progression driven by ITGA5$^+$ myofibroblasts and enhanced the efficacy of treatment with PD-L1 in a mouse model of HCC.

Conclusions Our findings elucidated a novel mechanism by which the EV-mediated transfer of ITGA5 from myofibroblasts to tumor cells augmented HCC stemness. ITGA5-targeting therapy helped prevent the progression of HCC and improved the efficacy of PD-L1 treatment.

Keywords Myofibroblasts, Integrin α5 (ITGA5), Extracellular vesicles (EVs), Hepatocellular carcinoma (HCC)

†Yang Xiao, Ping Tao and Keke Zhang contributed equally to this work.

*Correspondence:
Jian Hong
hongjian7@jnu.edu.cn
Chen Qu
Cheyne1988@outlook.com
Full list of author information is available at the end of the article

Graphical Abstract

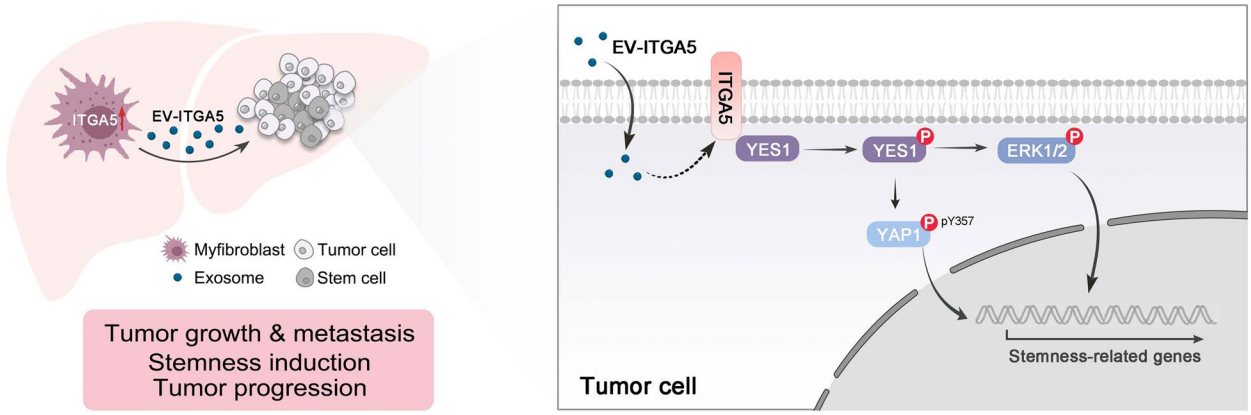

Introduction

Hepatocellular carcinoma (HCC) is an aggressive malignancy associated with poor survival globally. Surgical resection is the primary treatment option for HCC; however, the eligibility criteria for surgical resection limit its applicability to a select group of patients. Furthermore, approximately 50–70% of patients with HCC experience disease recurrence within 5 years following local regional therapy [1]. Although immune therapy has produced benefits, its therapeutic effect remains unsatisfactory for patients with advanced or recurrent HCC.

The tumor microenvironment (TME) plays a key role in the occurrence and development of malignancies [2]. As important components of the HCC TME, myofibroblasts play a significant role in HCC progression and recurrence [3, 4]. Hepatic myofibroblasts are identified by the expression of α-smooth muscle actin (α-SMA) and collagen type I [5]. Existing evidence suggests that myofibroblasts may primarily originate from activated hepatic stellate cells (HSCs) [6]. Myofibroblasts are absent in normal liver tissues. However, they are present in the fibrous scar tissues of chronically injured livers, where they contribute to the production of the extracellular matrix and the development of liver fibrosis [7]. The majority of patients with HCC have varying degrees of liver fibrosis, which enhances the infiltration of myofibroblasts in the HCC TME [8]. Myofibroblast infiltration in the TME promotes HCC progression through various mechanisms. Myofibroblasts enhance the proliferation, migration, invasion, and cancer stem cell-like (CSC-like) properties of HCC cells by secreting cytokines or extracellular vesicles (EVs) [8, 9].

Integrin is a type of heterodimeric transmembrane receptor mediating signal transduction between the intracellular and extracellular environments. The 18 α and 8 β subunits compose 24 integrins in humans, which participate in various biological activities such as hemostasis, differentiation, and immune responses [10, 11]. Integrin α5 (ITGA5) is a member of the integrin family, binding integrin β1 (ITGB1) to compose of α5β1 heterodimer [11]. Recent studies showed that ITGA5 plays a pivotal role in tumor growth, metastasis, and resistance to sorafenib in HCC [12–14]. Interestingly, we detected high expression levels of ITGA5 in myofibroblasts within the TME of HCC. However, the role of ITGA5 derived from myofibroblasts in HCC remains unclear. In this study, we explored the expression and localization of ITGA5 in the tumor microenvironment of HCC and investigated its role in promoting HCC progression.

Results

ITGA5+ myofibroblasts accumulate in HCC tissue and are associated with poor prognosis

Analysis of public data from The Cancer Genome Atlas (TCGA) and Gene Expression Omnibus (GEO; GSE14520) database indicated that the expression levels of ITGA5 were significantly higher in human HCC tissues than in adjacent non-tumorous liver tissues (Fig. 1A). Previous studies have shown that ITGA5 is crucial for predicting the prognosis of various malignant tumors [15–18]. In the present study, TCGA and GEO data analysis also suggested that high ITGA5 expression was linked to shorter overall survival (OS) and disease-free survival (DFS) in patients with HCC (Figs. S1A, B).

To further clarify the expression and localization of ITGA5 in HCC tissue, we performed an ITGA5 immunohistochemistry (IHC) assay on HCC tissues. IHC

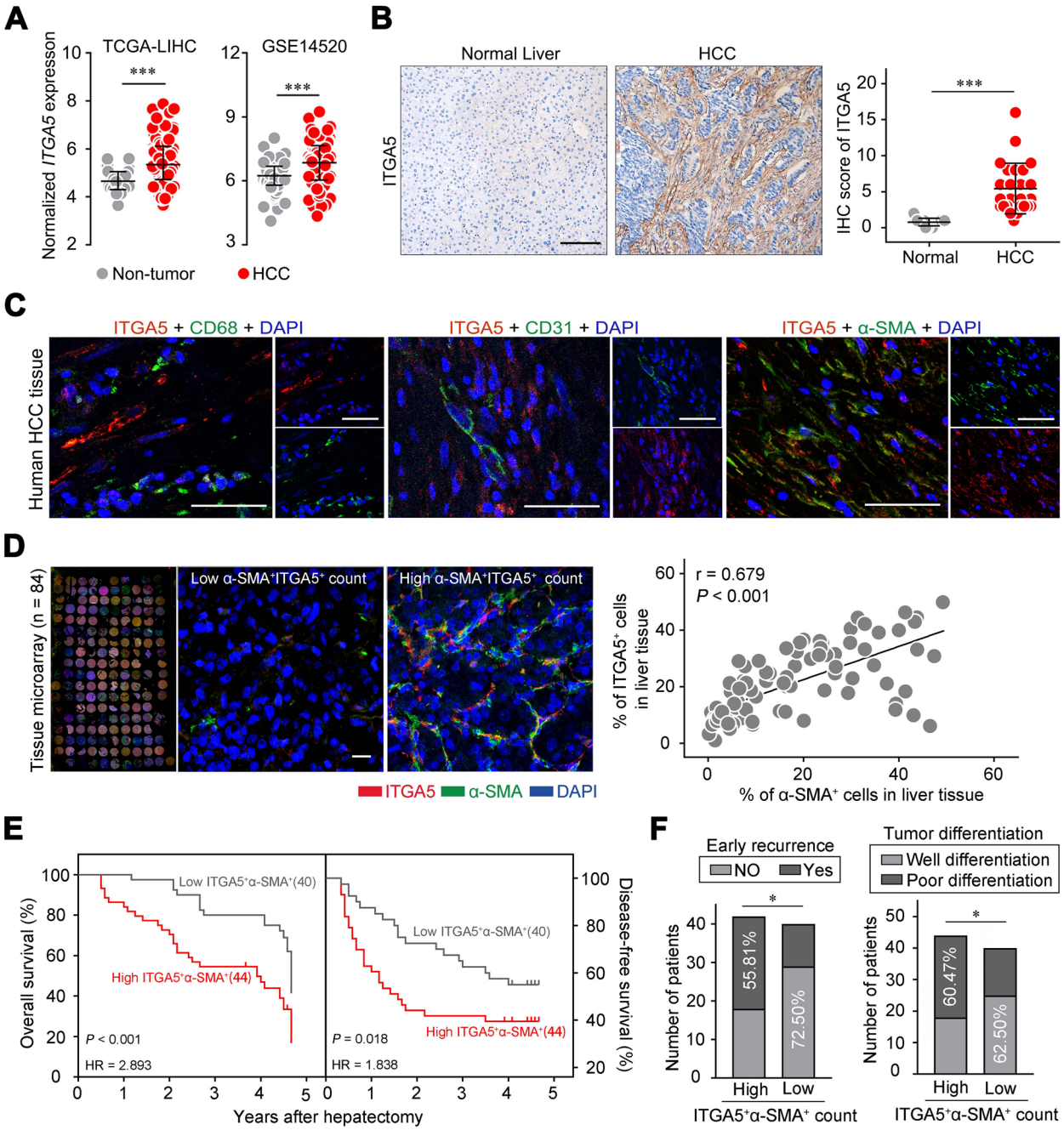

Fig. 1 ITGA5$^+$ myofibroblasts accumulated in HCC tissues and were associated with a poor prognosis. **A** Expression of ITGA5 mRNA in HCC and adjacent non-tumorous liver tissues (data from TCGA and GSE14520). **B** ITGA5 immunohistochemistry (IHC) staining of human normal liver and HCC tissues was performed. Representative images of ITGA5 IHC staining are shown in the left panel. The right panel shows the ITGA5 IHC scores of normal liver and HCC tissues. Scale bar: 50 μm. **C** Representative double immunofluorescence images of ITGA5 (red) with CD68 (green), CD31 (green), or α-SMA (green) in human HCC tissues. Scale bars: 50 μm. **D** Double immunofluorescence staining of α-SMA and ITGA5 in a tissue microarray including HCC tissues obtained from 84 patients with HCC. Representative images of HCC samples with high or low α-SMA$^+$ ITGA5$^+$ cell infiltration are shown in the left panel. The right panel shows the correlation analysis between the percentages of α-SMA$^+$ cells and ITGA5$^+$ cells in the TMA. Scale bar: 20 μm. **E** Overall survival (OS) and disease-free survival (DFS) curves of 84 HCC patients with high or low α-SMA$^+$ITGA5$^+$ cell infiltration. **F** The bar chart depicts the correlation between the infiltration levels of α-SMA$^+$ ITGA5$^+$ cells and early recurrence or tumor differentiation in 84 patients with HCC. *$P < 0.05$; ***$P < 0.001$

confirmed the upregulation of ITGA5 in HCC tissues (Fig. 1B). In addition, the results of the IHC assay suggested marked overexpression of ITGA5 in the stroma of HCC tissue versus normal liver tissues (Fig. 1B). To further investigate the special cellular localization of ITGA5 in the HCC stroma, multiplex immunofluorescence was performed. The results demonstrated that ITGA5 was located within the HCC stroma. This analysis revealed that ITGA5 predominantly localized to myofibroblasts (α-SMA$^+$) rather than macrophages (CD68$^+$) or endothelial cells (CD31$^+$) in human HCC tissues (Fig. 1C). The results indicated that ITGA5 would most likely accumulate in myofibroblasts within HCC tissues. Additionally, we identified co-localization of ITGA5 and α-SMA in both fibrotic and malignant liver tissues extracted from humans and model mice (Fig. S2). This observation suggested that an increase of ITGA5$^+$ myofibroblasts was associated with the dynamic processes of chronic liver injury and HCC development in the liver microenvironment. Furthermore, we detected ITGA5 expression in primary myofibroblasts from both the tumor and adjacent liver tissues of patients with HCC, whereas ITGA5 upregulation was noted in activated primary HSCs obtained from mice (Fig. S3). It is well established that activated HSCs are the primary source of myofibroblasts and that α-SMA expression increases continuously during HSC activation [19]. Our study revealed that ITGA5 was associated with increased α-SMA levels during HSC activation and maintained high expression levels in myofibroblasts (Figs. S3C, D). Moreover, ITGA5 expression was significantly higher in LX-2 cells (an activated HSC cell line) compared with HCC cell lines (Fig. S4A). Additionally, siRNA-mediated knockdown of ITGA5 suppressed the proliferation and activation of LX-2 cells (Figs. S4B–D). This evidence suggested that ITGA5 plays a role in regulating the activation of myofibroblasts.

We sought to further investigate the impact of ITGA5$^+$ myofibroblasts on HCC prognosis. Thus, dual immunofluorescence staining for α-SMA and ITGA5 was performed to examine the infiltration of ITGA5$^+$ myofibroblasts in a tissue microarray (TMA) of HCC tissues obtained from 84 patients with HCC. The results confirmed the colocalization of ITGA5 and α-SMA, and demonstrated that the number of ITGA5$^+$ cells was positively correlated with the number of α-SMA$^+$ cells (Fig. 1D). Further survival analysis based on the percentages of ITGA5$^+$ myofibroblasts (α-SMA$^+$ITGA5$^+$ cells) indicated that high ITGA5$^+$ myofibroblast infiltration was correlated with shorter OS (hazard ratio: 2.893, $P<0.001$) and DFS (hazard ratio: 1.838, $P=0.018$) (Fig. 1E). In addition, the results suggested that high ITGA5$^+$ myofibroblast infiltration was associated with poor differentiation and early recurrence in HCC (Fig. 1F). Increased ITGA5$^+$ myofibroblasts in poorly differentiated HCC samples correlated with a higher risk of shorter OS (Fig. S5).

ITGA5 knockdown abolishes the myofibroblast-induced stemness enhancement of HCC cells

Activated HSCs are one of the primary sources of myofibroblasts in the TME of HCC. Therefore, in this study, we used the activated HSC line LX-2 to construct a myofibroblast-HCC cell co-culture model. Using this model, we investigated the role of ITGA5 in the process by which myofibroblasts promote HCC progression.

Studies have demonstrated the HCC-promoting effect of myofibroblasts [8]. To investigate the role of ITGA5 in the tumor-promoting function of myofibroblasts, we performed RNA-sequencing on Huh7 cells cultured with conditioned medium (CM) from myofibroblasts (TGF-β1-induced LX-2 cells) with or without ITGA5 knockdown. RNA sequencing revealed 418 differentially expressed genes between Huh7 cells treated with CM from LX-2 cells with or without ITGA5 knockdown (Fig. 2A). Gene Ontology (GO) enrichment analysis indicated that the differentially expressed genes were associated with several GO terms, including cell differentiation, cell migration, and cell death functions (Fig. 2B). Gene Set Enrichment Analysis (GSEA) showed that genes related to the negative regulation of stem cell proliferation were enriched in the Huh7 cells treated with CM from ITGA5-knockdown LX-2 cells, whereas integrin-mediated

(See figure on next page.)

Fig. 2 Enhancement of stemness in HCC cells induced by myofibroblasts was abolished after the knockdown of ITGA5. **A** Volcano plot showing the differentially expressed genes (DEGs) detected by RNA-sequencing (RNA-seq) in Huh7 cells cultured with conditioned medium (CM) from myofibroblasts (TGF-β1 induced LX-2 cells) with or without ITGA5 knockdown (si-Ctrl CM *vs.* si-ITGA5 CM). **B** GO enrichment analysis of DEGs. **C** The GSEA revealed several signaling pathways that were notably enriched among the DEGs. **D** Sphere formation assays were conducted in Huh7 cells with CM of myofibroblasts (si-Ctrl or si-ITGA5). Scale bar: 50 μm. **E** Schematic of the subcutaneous xenograft mouse model injected with Huh7 cells alone or co-injected with myofibroblasts (vector or ITGA5-KO). **F** Variation in tumor volume among the indicated groups. **G** Quantification of the tumor weights in the indicated groups ($n=6$ for each group). **H** Respective IHC staining images and quantification of ITGA5 and EPCAM in the tumor tissues of the indicated groups. Scale bar: 50 μm. **I** Representative immunofluorescence images of ITGA5 (red), α-SMA (green), and ALDH (pink) in human normal liver tissue or HCC tissues. Scale bar: 50 μm. *$P<0.05$; **$P<0.01$; ***$P<0.001$. Data were obtained from three independent experiments per group

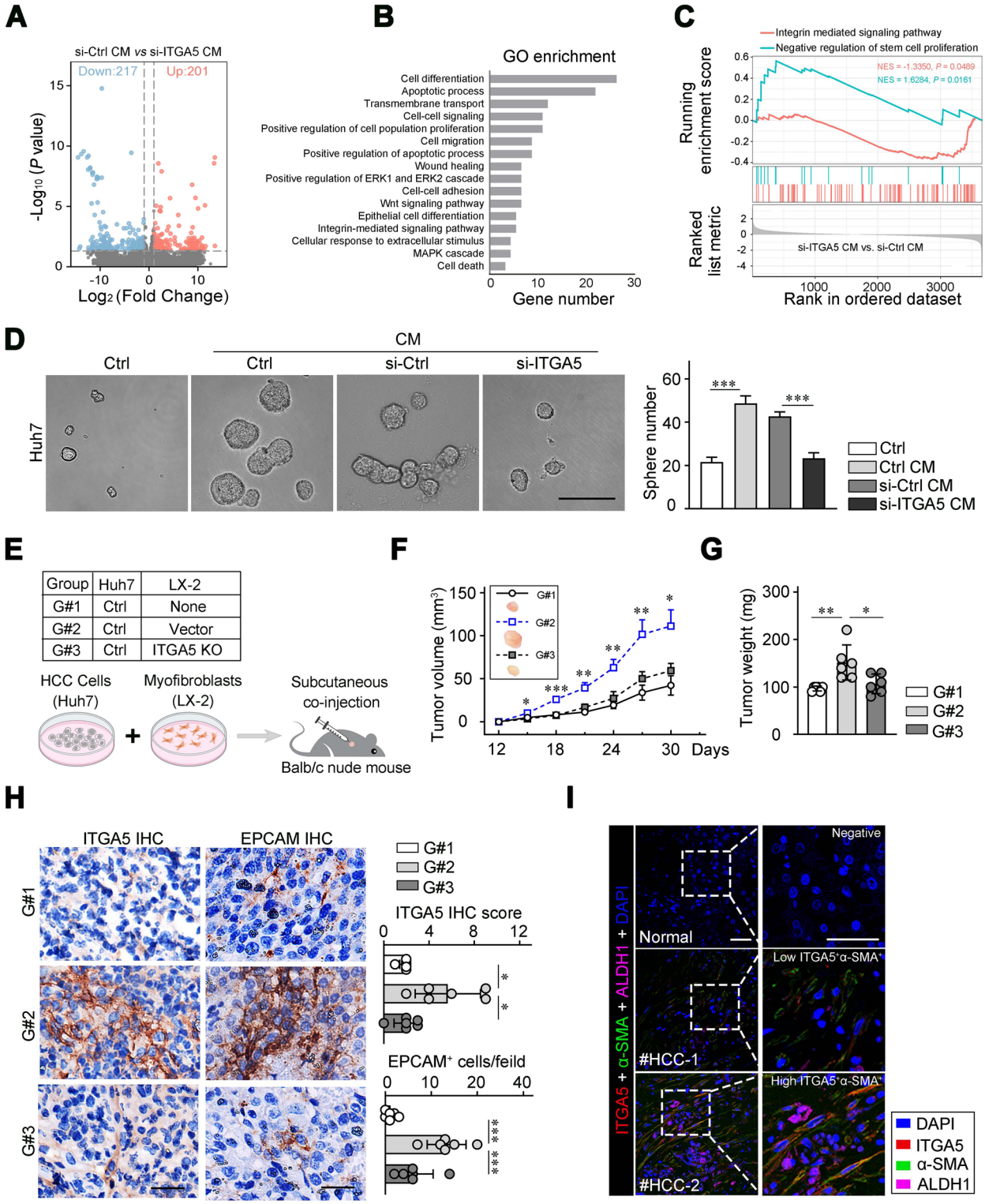

Fig. 2 (See legend on previous page.)

signaling was enriched in Huh7 cells treated with LX-2 CM (Fig. 2C). Previous studies have reported that myofibroblasts promoted the CSC properties of HCC cells [8, 20]. These results suggested that ITGA5 regulated the myofibroblast-induced promotion of CSC-like properties in HCC cells. Further sphere-forming assays confirmed that CM of LX-2 cells enhanced the sphere-forming ability of Huh7 cells, whereas ITGA5 knockdown in LX-2 cells reversed this effect (Fig. 2D).

Subsequently, we established a subcutaneous xenograft mouse model to investigate the function of myofibroblast ITGA5 in tumor promotion. The results suggested that the co-injection of myofibroblasts and HCC cells accelerated growth and increased the expression of the CSC biomarker (epithelial cell adhesion molecule [EPCAM]) compared with the injection of HCC cells alone. However, ITGA5 deficiency in myofibroblasts abolished these effects (Fig. 2E–H). Additionally, we observed that ALDH1, a CSC biomarker-positive HCC cells mainly surrounded ITGA5$^+$ α-SMA$^+$ myofibroblasts in human HCC tissues (Fig. 2I). On the other hand, we detected an increased number of ALDH-positive HCC cells in HCC tissues with high ITGA5$^+$ α-SMA$^+$ cells infiltration compared to HCC tissues with low ITGA5$^+$ α-SMA$^+$ cells infiltration (Fig. 2I). These results suggested that ITGA5$^+$ myofibroblasts facilitated HCC stemness.

Myofibroblast-derived EVs facilitate ITGA5 transfer to HCC cells and enhance the stemness of HCC cells

Interestingly, our results also showed that the protein expression of ITGA5 was upregulated in HCC cells after treatment with CM derived from LX-2 cells (Fig. 3A–C). Moreover, silencing ITGA5 expression in LX-2 cells abolished this effect (Fig. 3A–C). This finding suggested that myofibroblasts transmit ITGA5 to HCC cells through a component in the CM. Existing evidence suggests that EVs play a crucial role in mediating intercellular protein transfer [21]. Therefore, we used the EV inhibitor GW4869 to investigate whether inhibiting vesicle formation could block the LX-2 CM-mediated increase of ITGA5 protein levels in HCC cells. The results showed that, after inhibiting EV production, LX-2 CM lost the ability to upregulate ITGA5 protein expression in HCC cells (Fig. 3B, D). To further confirm the role of myofibroblast-derived EVs in ITGA5 transfer, we isolated and purified EVs from LX-2 CM and used them to treat HCC cells (Fig. 3E). The results revealed that treatment with LX-2 EVs upregulated ITGA5 protein expression in HCC cells in a concentration- and time-dependent manner (Fig. 3G). However, there was no difference in ITGA5 mRNA expression in the EV-treated group (Fig. 3F). Besides, we established over expression of Flag-tagged ITGA5 in LX-2 cells to collect the EVs, which were then used to treat Huh7 cells. We found that the Flag-tag could be detected in huh7 cells treated with EVs from LX-2 cells transfected with Flag-ITGA5 virus. (Fig. S6A, 6B). These findings indicated that myofibroblasts transmitted ITGA5 to HCC cells through EVs. Additionally, we further investigated the role of myofibroblast-derived EVs in regulating the stemness of HCC cells. The results showed that blocking the generation of EVs in LX-2 cells abolished the LX-2 CM-mediated enhancement of HCC cell stemness (Fig. 3H). Moreover, treatment of HCC cells with isolated LX-2 EVs also enhanced the stemness of HCC cells (Fig. 3H). Furthermore, the overexpression of ITGA5 in HCC cells also enhanced the stemness of HCC cells (Fig. S7). These findings suggested that myofibroblasts enhanced the stemness of HCC cells by transmitting ITGA5 via EVs.

ITGA5 depletion in myofibroblasts abolishes myofibroblast-derived EV-mediated ITGA5 transfer and stemness enhancement

We sought to determine whether ITGA5 derived from myofibroblast EVs plays a crucial role in HCC stemness. Therefore, we utilized a CRISPR-Cas9 system to establish ITGA5-knockout (ITGA5-KO) LX-2 cells, and isolated EVs from those cells. We examined the expression of ITGA5 in whole-cell lysates and EVs from LX-2 cells with or without ITGA5-KO. We found that ITGA5 was scarcely present in both the cell lysates and EVs of ITGA5-KO LX-2 cells (Fig. 4A). Additionally, our results indicated that ITGA5-KO abolished EV-mediated upregulation of ITGA5 proteins in HCC cells (Fig. 4B, C). Specifically, the protein levels of ITGA5 were higher in HCC cells treated with EVs (vector EVs) than in ITGA5-lacking EVs (ITGA5-KO EVs)-treated cells or only phosphate-buffered saline-treated cells (vehicle). Thereafter, spheroid formation assays were conducted to investigate the self-renewal ability of HCC cells (Huh7 or PLC/PRF/5) pretreated with ITGA5-EVs or ITGA5-KO EVs. The results showed that the number of spheroids in HCC cells treated with ITGA5-EVs increased significantly, whereas ITGA5-KO EVs mitigated this effect in both the first and second passages of sphere formation (Fig. 4D, E). Furthermore, the expression of key CSC markers MYC, SOX2, and EPCAM, was enhanced in HCC cells after treatment with ITGA5-EVs. However, this effect was also abolished by ITGA5-KO in myofibroblasts (Fig. 4F, G). The tumorigenesis and self-renewal capabilities were further assessed through serial transplantation of primary xenografts into secondary mouse recipients. This experiment revealed that HCC cells treated with ITGA5-enriched EVs exhibited a marked increase in tumorigenicity, accompanied by higher tumor incidence, shorter tumor latency, and reduced tumor-free survival compared with

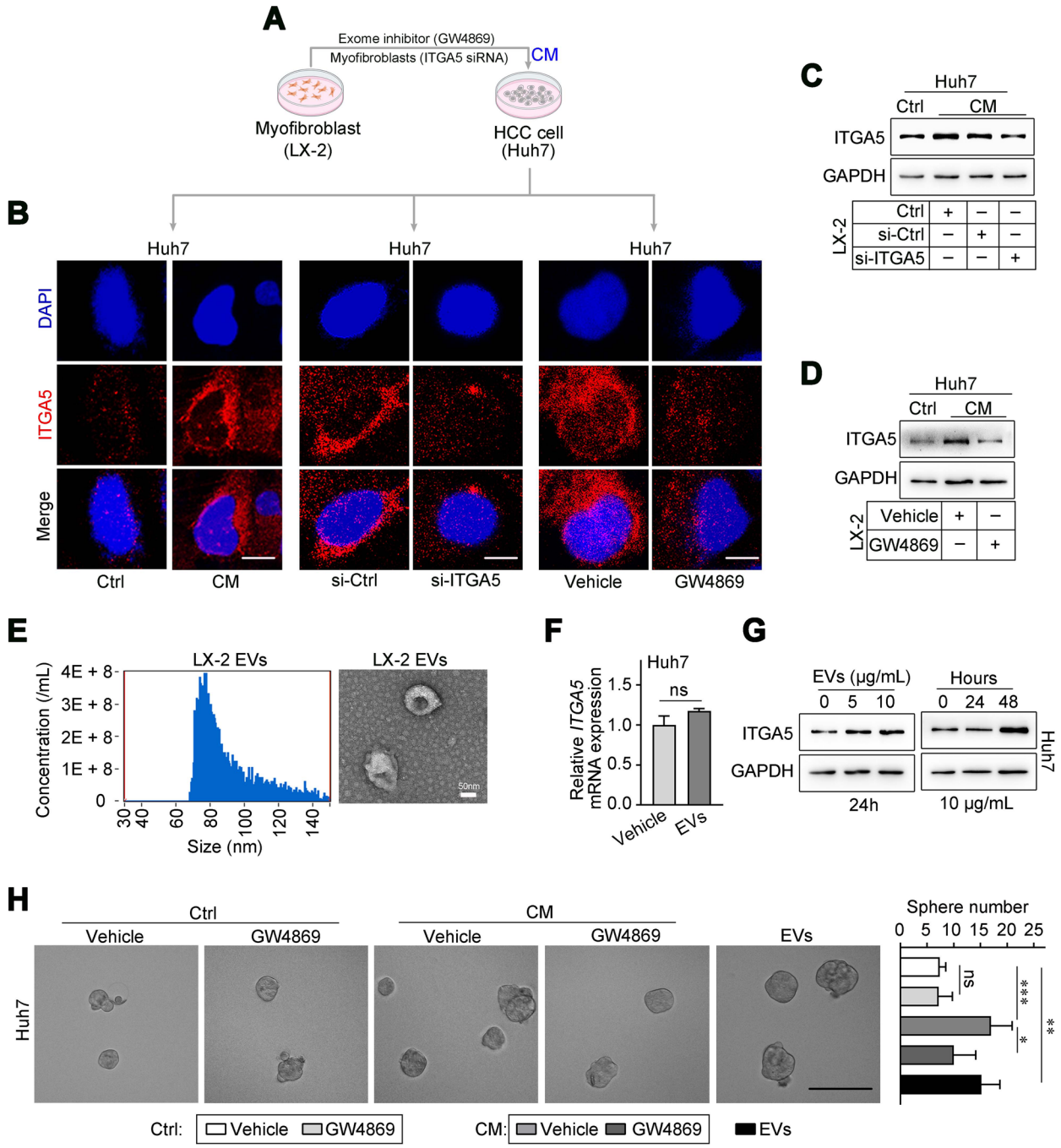

Fig. 3 EV-mediated ITGA5 transfer from myofibroblasts to HCC cells enhanced the stemness of HCC cells. **A** Schematic of the in vitro experiment depicting HCC cells (Huh7) cultured with conditioned medium (CM) from myofibroblasts (LX-2 cells with the indicated treatment). **B** Representative immunofluorescence images of ITGA5 (red) in Huh7 cells treated with or without CM of LX-2 cells (si-Ctrl, si-ITGA5, or treated with GW4869). Scale bars: 20 μm. **C** Immunoblotting of ITGA5 in Huh7 cells treated with or without CM of LX-2 cells (si-Ctrl or si-ITGA5). **D** Immunoblotting of ITGA5 in Huh7 cells cultured with or without LX-2 cells (treated with GW4869 or not). **E** Nanoparticle tracking analysis of LX-2 EVs (left panel); representative transmission electron microscopy image of LX-2 EVs (right panel). Scale bar: 50 nm. **F** Relative mRNA expression of ITGA5 in Huh7 cells treated with EVs or not. **G** Immunoblotting of ITGA5 in Huh7 cells treated with 0, 5, or 10 μg/mL EVs for 24 h, or with 10 μg/mL EVs for 0, 24, or 48 h. **H** Sphere formation assay of Huh7 cells subjected to the indicated treatment. Scale bar: 100 μm. *$P < 0.05$; **$P < 0.01$; ***$P < 0.001$. All data were obtained from three independent experiments per group

HCC cells treated with ITGA5-KO EVs (Fig. 4H–J). Moreover, IHC staining confirmed that ITGA5-EVs significantly increased Ki67 and EPCAM expression in subcutaneous xenografts, whereas ITGA5-KO EVs mitigated these effects (Fig. 4K). We also examined whether ITGA5 affected the enhancement of the proliferation and invasiveness of HCC cells mediated by myofibroblasts. We found that HCC cells treated with myofibroblasts CM or EVs presented a significant increase in colony number compared with untreated control cells. Notably, the depletion of ITGA5 in myofibroblasts reduced this effect (Fig. S8). Similarly, ITGA5 knockdown or ITGA5-KO in myofibroblasts also attenuated the enhanced migration and invasion capacity of HCC cells induced by treatment with CM or EVs derived from myofibroblasts in vitro and in vivo (Fig. S9).

ITGA5 enhances the stemness phenotypes of HCC cells via interacting with and activating YES1

To investigate the mechanism by which ITGA5 enhances the CSC properties of HCC cells, Huh7 cells were transfected with Flag-ITGA5 lentivirus or vector control. Flag co-immunoprecipitation/mass spectrometry (Co-IP/MS) was performed to identify ITGA5-interacting proteins. We identified 288 ITGA5-interacting proteins via Co-IP assays. Of those, 23 proteins were related to stemness signaling (Fig. 5A). Among these 23 proteins, YES1 (a non-receptor tyrosine kinase of Src family kinases [SFKs]) strongly interacted with ITGA5 (Fig. 5B). Co-IP/western blotting assays and molecular docking further confirmed the interaction between ITGA5 and YES1 (Fig. 5C, D). In addition, molecular docking suggested that the cytoplasmic tail domain of ITGA5 was the binding site for YES1 (Fig. 5D). Thus, we constructed an ITGA5-truncated variant (Δ1022–1049) plasmid to confirm this interaction (Fig. 5E). Co-IP assays confirmed that the cytoplasmic tail domain was necessary for the interaction between ITGA5 and YES1 (Fig. 5F). These results demonstrated the direct interaction between ITGA5 and YES1. Moreover, we found that overexpression of the wild-type ITGA5 promoted the phosphorylation and activation of YES1, whereas overexpression of mutated ITGA5 (Δ1022–1049) did not affect YES1 phosphorylation (Fig. 5G). Here, we used pY416 Src family kinase (SFK) antibody to detect the phosphorylation and activation of YES1. YES1 is a member of the Src family kinase (SFK). And pY416 SFK antibody is commonly accepted to evaluate the activation YES1 [22]. YES1 activation was previously linked to the phosphorylation and activation of downstream YAP1 and ERK1/2 signaling, which were involved in cancer stemness [23–25]. Our findings also showed that overexpression of wild-type ITGA5, but not mutated ITGA5, promoted the phosphorylation and activation of ERK1/2 and YAP1 (Fig. 5G).

Additionally, we investigated the impact of LX-2-derived ITGA5-enriched EVs on YES1 and its downstream ERK1/2 and YAP1 pathways. The results showed that treatment with ITGA5-enriched EVs promoted the phosphorylation and activation of YES1 and its downstream targets ERK1/2 and YAP1 in HCC cells (Fig. 5H). This effect was accompanied by an increase in the nuclear localization of YAP1 (Fig. 5I). We also found that blocking ITGA5 by an ITGA5 inhibitor AV3 (Fig. S9A) or using YES1 inhibitor CH6953755 reversed the ITGA5-EV-mediated activation of ERK1/2 and YAP1 (Figs. 5H, I). These findings suggested that ITGA5 promotes the phosphorylation and activation of YES1 through direct interaction, thereby activating the downstream ERK and YAP pathways. In addition, blocking ITGA5 or treatment with a YES1 inhibitor abolished the EV-induced stemness enhancement in HCC cells. Obviously, the increased expression of CSC markers (MYC, EPCAM, SOX2) and the self-renewal ability of HCC cells treated with EVs were suppressed by ITGA5 or YES1 inhibitor (Figs. 5H, J). These findings supported that ITGA5 interacts with YES1 to activate ERK1/2 and YAP1 and enhance the CSC-like phenotype in HCC cells.

(See figure on next page.)

Fig. 4 ITGA5 depletion in myofibroblasts abolished myofibroblast-derived EV-mediated ITGA5 transfer and stemness enhancement. **A** Immunoblotting of ITGA5 in whole cell lysate of LX-2 cells (vector or ITGA5-KO) and EVs derived from LX-2 cells (vector or ITGA5-KO). **B** Immunoblotting of ITGA5 in HCC cells treated with or without EVs from LX-2 cells (vector or ITGA5-KO). **C** Representative images of ITGA5 immunofluorescence in Huh7 cells treated with or without EVs from LX-2 cells (vector or ITGA5-KO). Scale bar: 20 μm. **D**, **E** Spheroid formation of Huh7 cells and PLC/PRF/5 cells treated with or without EVs from LX-2 cells (vector or ITGA5-KO) at primary (P1) and secondary (P2) passage. Scale bar: 100 μm. **F** Representative immunofluorescence images of EPCAM in Huh7 cells and PLC/PRF/5 cells treated with or without EVs from LX-2 cells (vector or ITGA5-KO). Scale bar: 20 μm. **G** Immunoblotting of ITGA5 and CSC markers (MYC, EPCAM, and SOX2) in Huh7 or PLC/PRF/5 cells subjected to the indicated treatment. **H** Images of tumors formed by Huh7 cells pretreated with or without the indicated EVs after two rounds of implantation ($n = 5$ per group). **I** Tumor-free survival curves of mice injected with Huh7 cells during the primary and secondary implantation are shown. **J** Percentages of tumorigenesis in the indicated groups after primary and secondary implantation. **K** IHC staining of Ki67 and EPCAM in xenografts from indicated groups ($n = 5$ per group). Scale bar: 50 μm. $^{**}P < 0.01$; $^{***}P < 0.001$. All data were obtained from three independent experiments per group

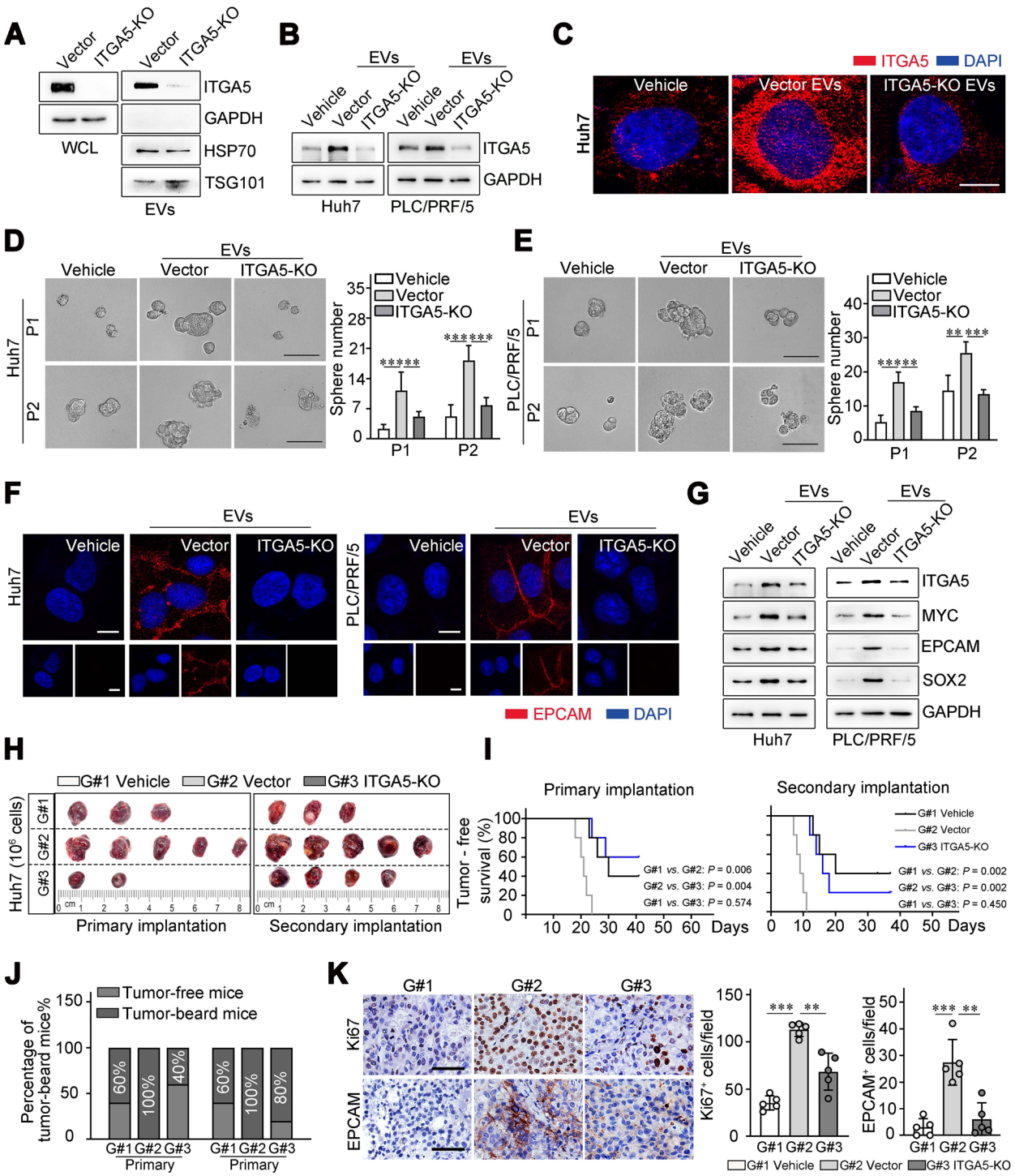

Fig. 4 (See legend on previous page.)

ITGA5 blockade ameliorates the progression of HCC in vivo

To investigate the therapeutic potential of targeting ITGA5 in HCC, a novel ITGA5-targeting peptidomimetic AV3 (Fig. S10A) was administered in vitro and in vivo. In vitro binding studies with 5-carboxyfluorescein (5FAM) conjugated AV3 showed stronger binding to ITGA5-EV-treated HCC cells versus untreated HCC cells (Fig. S10B). Moreover, AV3 effectively inhibited the proliferation and sphere formation of HCC cells induced by ITGA5-EVs (Figs. S10C, D), and decreased the expression

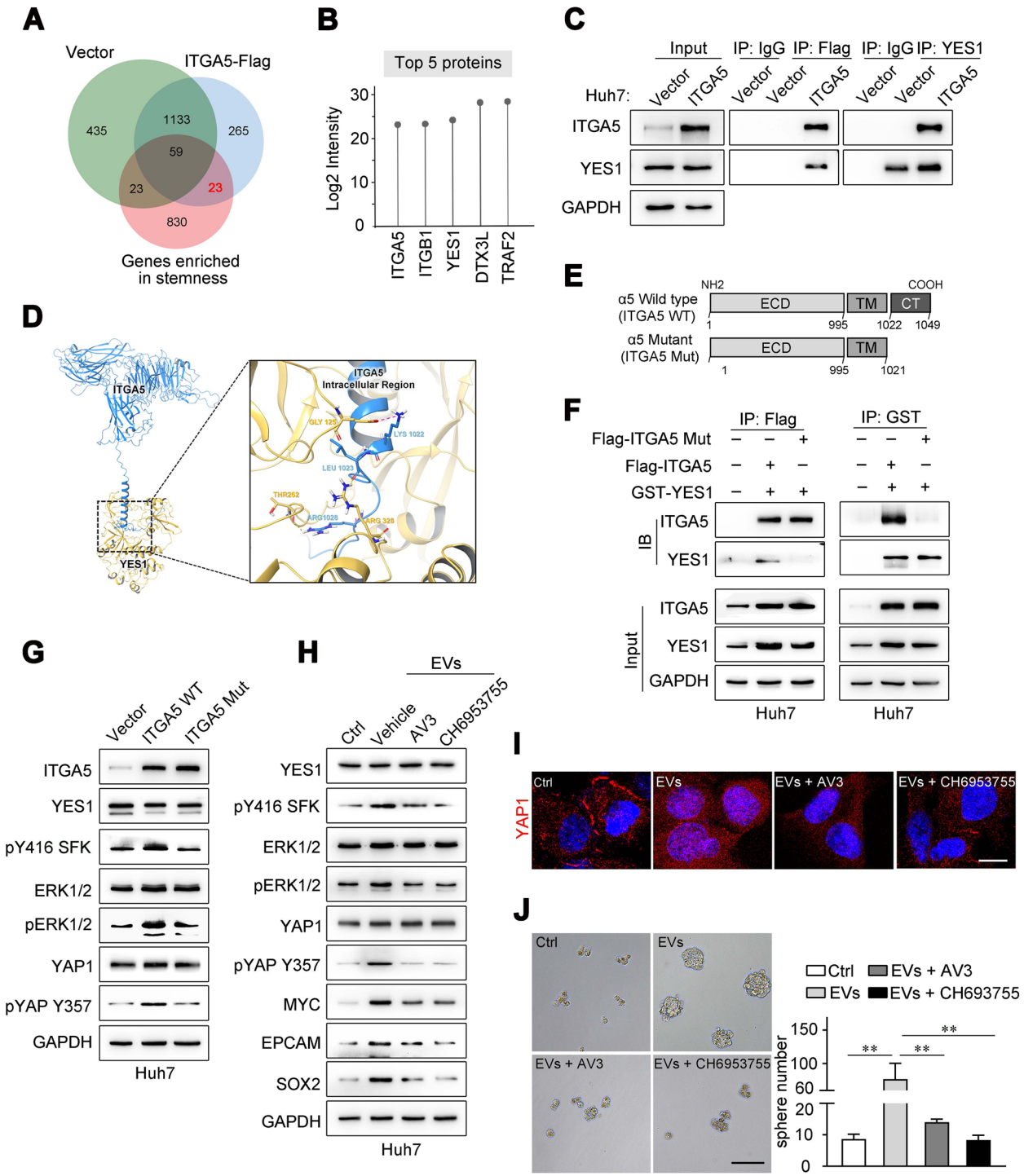

Fig. 5 ITGA5 enhanced the stemness phenotypes of HCC cells via interacting with and activating YES1. **A** Venn diagram showing the ITGA5-interacting tumor stemness-related proteins identified by mass spectrometry. **B** The top five unique ITGA5-interacting tumor stemness-related proteins. **C** Co-IP confirmed the interaction between ITGA5 and YES1. **D** Molecular docking of the interaction between ITGA5 and YES1. **E** Schematic of wild-type and mutant ITGA5. **F** Co-IP assays were performed using anti-Flag beads and GST antibodies in Huh7 cells co-transfected with Flag-ITGA5 WT/GST-YES1 or Flag-ITGA5 mutation/GST-YES1 plasmids. **G** Immunoblotting of Huh7 cells subjected to the indicated treatment. **H** Immunoblotting of Huh7 cells subjected to the indicated treatment. **I** Representative immunofluorescence images of YAP1 in Huh7 cells subjected to the indicated treatment. Scale bar: 20 μm. **J** Spheroid formation of Huh7 cells subjected to the indicated treatment. Scale bar: 100 μm. $^{**}P < 0.01$. All data were obtained from three independent experiments per group

of the CSC markers MYC, EPCAM, and SOX2 in EV-treated HCC cells (Fig. S10E).

Our previous study revealed the presence of few myofibroblasts in orthotopically implanted HCC tissues obtained from mice with a normal liver [26]. Importantly, pretreatment with carbon tetrachloride (CCl_4) gavage significantly enhanced myofibroblast infiltration in orthotopically implanted HCC tissue [26]. To simulate the infiltration of myofibroblasts and investigate the function of ITGA5$^+$ myofibroblasts in HCC development, we established an orthotopic HCC model in mice with CCl_4 gavage pretreatment (Fig. 6A). In this orthotopic HCC mouse model, we found that AV3 treatment significantly suppressed HCC growth without affecting body weight (Fig. 6B–D). Moreover, IHC staining showed that ITGA5 treatment significantly reduced the expression of the CSC marker EPCAM in orthotopic HCC tissues (Fig. 6E). This evidence confirmed that ITGA5 blockade reduced the stemness of HCC cells. Interestingly, our results also suggested that the number of ITGA5$^+$ and α-SMA$^+$ cells was decreased in HCC tissues extracted from AV3-treated mice (Fig. 6E). The data indicated that ITGA5 blockade also reduced ITGA5$^+$ myofibroblast infiltration in HCC tissues.

Inhibition of ITGA5 enhances the efficacy of PD-L1 blockade treatment

Although PD-1 or PD-L1 blockade treatment have become an important treatment option for advanced HCC, only 20–30% of patients respond to this therapy. Increasing evidence indicated that myofibroblasts or cancer-associated fibroblasts regulated the tumor immune microenvironment and affected the treatment effect of PD-1 or PD-L1 blockade treatment [27, 28].

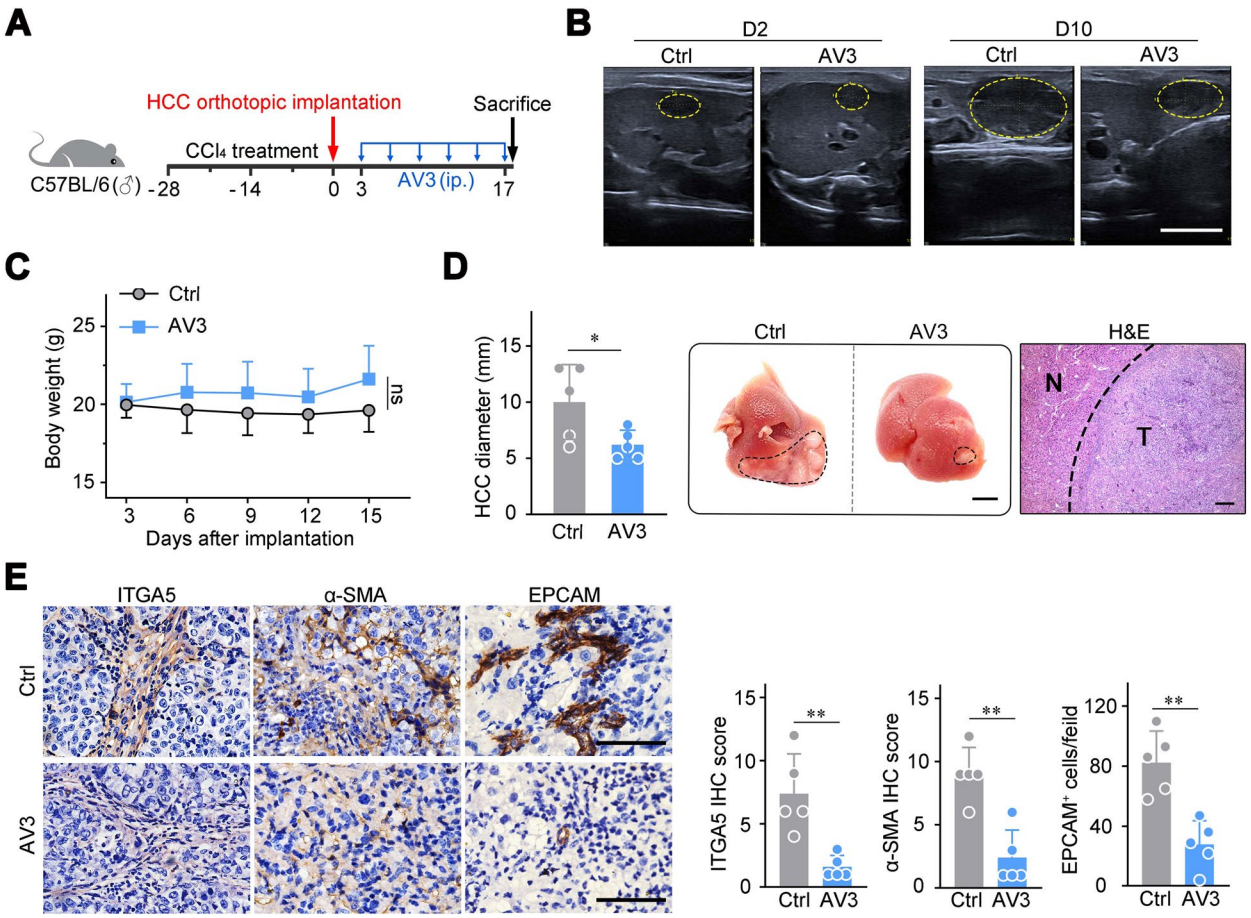

Fig. 6 ITGA5 blockade ameliorated the progression of HCC in vivo. **A** Schematic representation of the establishment of the orthotopic HCC mouse model. Mice were subjected to gavage with CCl_4 for 4 weeks, followed by HCC implantation and ITGA5 blockade (AV3) treatment ($n = 5$ per group). **B** Ultrasonography of HCC mice at 2 and 10 days after HCC implantation. Scale bar: 5 mm. **C** Weights of the HCC mice in both groups. **D** Quantification of the tumor diameter and representative images of the orthotopically implanted tumors in the indicated groups. Scale bar: 0.5 cm (middle panel); 100 μm (right panel). **E** ITGA5, α-SMA, and EPCAM were detected by IHC in orthotopically implanted tumors from the indicated groups. Scale bar: 50 μm. *$P < 0.05$; ***$P < 0.001$

Our bioinformatics analysis revealed that ITGA5 expression was correlated with cancer-associated fibroblast infiltration, stromal score, immune cell infiltration, and immune checkpoint-related gene expression (Fig. S11). It suggested that ITGA5 influences the efficacy of ICIs. Thus, we utilized the CCl_4 pretreatment orthotopic HCC mouse model to investigate whether inhibiting ITGA5 enhanced the therapeutic efficacy of ICIs (Fig. 7A).

To evaluate the role of ITGA5 blockade in improving ICI therapeutic efficacy, mice were treated with immunoglobulin G (IgG), saline, the ITGA5 inhibitor AV3, a PD-L1 antibody, or a combination of a PD-L1 antibody and AV3. Bioluminescent imaging indicated that 2 days after HCC implantation, the tumors could be detected. Of note, there was no significant difference in luminescence intensity among these groups. However, 10 days after HCC implantation, the luminescence intensity of orthotopic HCC in combination-treated mice was significantly lower than that recorded in mice that received anti-PD-L1 or AV3 treatment (Fig. 7B, C). AV3 and PD-L1 antibody combination treatment also significantly prolonged the survival time of the orthotopic HCC mice compared with AV3 or anti-PD-L1 monotherapy (Fig. 7D). In addition, the autopsy results indicated that the combination therapy of AV3 and anti-PD-L1 significantly reduced the incidence of intrahepatic metastasis (Fig. 7E).

Some orthotopic HCC mice were sacrificed 2 weeks after orthotopic HCC implantation to further confirm the anti-HCC effect of the combination therapy. The results also suggested that combination therapy with AV3 and anti-PD-L1 could better control HCC progression than treatment with AV3 or anti-PD-L1 alone (Fig. 7F, G). To evaluate the impact of AV3 on the HCC TME, we assessed the infiltration of TME cells through multiplex immunofluorescence and IHC. Monotherapy and combination therapy both impaired myeloid-derived suppressor cells (MDSCs [$CD11b^+Gr1^+$ positive cells]) and tumor-associated macrophage infiltration. However, the combination therapy significantly increased $CD8^+$ and $CD4^+$ T cell infiltration. Notably, only AV3 monotherapy and combination therapy remarkably decreased the infiltration of $ITGA5^+$ myofibroblasts ($ITGA5^+\alpha\text{-SMA}^+$ cells) (Figs. 7H, S12, S13). In addition, we compared the infiltration of M1 macrophages and M2 macrophages in the tumor tissues of mice in each group. The results showed that targeting ITGA5 enhanced the inhibitory effect of PD-L1 on M2 macrophages; however, it did not exert a significant effect on M1 macrophages (Figs. 7H, S13, S14). These findings implied that the ITGA5 blockade-induced enhancement of PD-L1 blockade treatment efficacy may be achieved through modulation of the TME.

Discussion

The TME plays a crucial role in the initiation and progression of HCC. Myofibroblasts, the main stromal cells within the HCC TME, promote HCC progression. Evidence suggests that myofibroblasts enhance HCC proliferation, metastasis, and resistance to therapy through paracrine signaling [8, 9, 29, 30]. However, the detailed molecular mechanisms underlying these effects remain partly understood.

ITGA5 is a member of the integrin family, a group of transmembrane receptors that mediate signal transduction between cells and their external environment, including the extracellular matrix [31, 32]. Integrins play a pivotal role in signal transduction within the microenvironment and are crucially involved in the progression of various diseases, including tumors, cardiovascular disorders, and immune-related conditions [33–35]. In particular, ITGA5 has been implicated in fibrotic disorders, and cancers [8, 29]. Previous studies have shown that ITGA5 in cancer cells contributes to the regulation of invasion and metastasis in malignancies such as breast, pancreatic, and gastric cancer [14, 15, 30].

Existing studies have shown that high ITGA5 expression is associated with poor prognosis of HCC [12], and ITGA5 enhances the malignant phenotypes (e.g., proliferation, invasion, and metastasis) of HCC cells [12]. However, its expression and molecular function in the TME of HCC are not yet fully understood. This study found that ITGA5 is primarily expressed in myofibroblasts within the TME of HCC, and these cells can transfer ITGA5 into HCC cells via EVs, thereby regulating the malignant phenotype of HCC cells. EVs are nanoscale

(See figure on next page.)

Fig. 7 Inhibition of ITGA5 enhanced the efficacy of PD-L1 treatment in HCC. **A** Schematic of the design of ITGA5 inhibitor and immune checkpoint inhibitor treatments in an orthotopic HCC model established in mice pretreated with CCl_4. **B** Bioluminescence imaging on days 2 and 10 in orthotopic HCC model mice subjected to the indicated treatments ($n=4$). **C** Quantification of the bioluminescence signal. **D** OS curves of orthotopic HCC model mice following the indicated treatments. **E** Intrahepatic metastasis rates in each group. **F** Representative image of livers obtained from the indicated groups. Scale bar: 0.5 cm. **G** Quantification of the tumor diameter in the indicated groups. **H** Representative immunofluorescence images of ITGA5 (red)/α-SMA (green) and CD11b (green)/CD206 (red)/CD4 (gray)/CD8 (cyan) in orthotopic HCC tissues extracted from the indicated groups. Scale bar: 50 μm. $^*P<0.05$; $^{**}P<0.01$; $^{***}P<0.001$

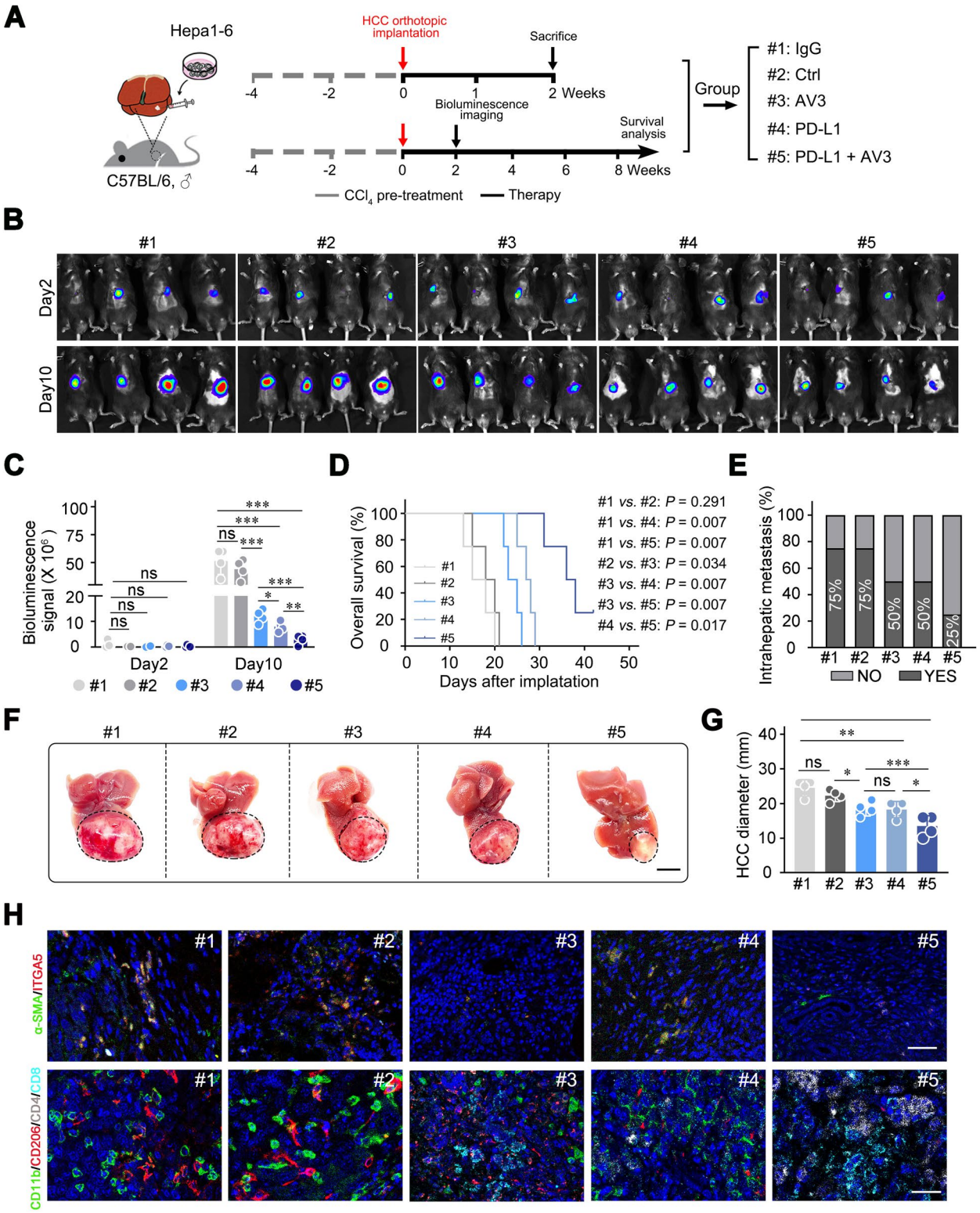

Fig. 7 (See legend on previous page.)

vesicles produced by various cells that can transfer bioactive molecules, such as lipids, nucleic acids, and proteins, from donor cells to recipient cells. Increasing evidence suggests that, beyond regulation by direct cellular contact and soluble factors, EVs play a critical role in cell–cell communication during tumor progression [36, 37]. Certain TME cells, such as myofibroblasts, can produce EVs to transfer relevant molecules into tumor cells, thus exerting regulatory effects on these cells [38]. Despite reports on the intercellular transfer of integrins via EVs, whether ITGA5 can be transferred to HCC cells via EVs and exert regulatory effects remains uncertain.

In the present study, we found that ITGA5 can be transferred from myofibroblasts to HCC cells through myofibroblast-derived EVs. Following transfer into HCC cells, ITGA5 significantly enhances the stemness of HCC cells and promotes their proliferation and invasiveness/metastasis. Mechanistically, the findings indicated that ITGA5-mediated CSC-like properties of HCC cells were dependent on interacting with and activating YES1. YES1, a member of the Src kinase family, is thought to be mainly activated through conformational changes that induce autophosphorylation, thereby promoting phosphorylation of downstream proteins, such as YAP1, and activating related pathways [24, 39]. Our findings suggested that the interaction between ITGA5 and YES1 may promote YES1 conformational changes and autophosphorylation activation, though further research is needed to confirm this mechanism. Some studies pointed out that, in colorectal cancer, YES1 induced stemness and resistance to chemotherapy by promoting YAP1 activation and nuclear translocation. YES1 can also induce resistance in melanoma by activating the ERK signaling pathway [40]. In our study, activation of YES1-driven downstream pathways, including YAP1 and ERK1/2, has been closely associated with enhanced stemness of tumor cells. Particularly, the treatment of ITGA5 inhibitors can block the enhancement of HCC cell stemness by suppressing the activation of the YES1 pathway and the downstream signaling. Moreover, ligands and extracellular region may also be essential for ITGA5 to exert its molecular biological functions. It had been reported that the activation of integrins depends on their binding to extracellular ligands, such as fibronectin, fibrinogen, and the cytokine receptor, which in turn triggers conformational changes to induce the transmission of intracellular downstream signaling [11, 41]. The absence of ligands or the extracellular region may affect the molecular function of ITGA5. However, further experiments are needed for verification. Other research proved that ITGA5 typically needs to dimerize with ITGB1 and bind to its ligand fibronectin to exert its functions [14, 42]. We also explored whether ITGB1 participates in the ITGA5-induced HCC stemness. We found that interfering with ITGB1 expression impaired the ITGA5-induced enhancement of stemness in HCC cells (Fig. S15). Nevertheless, further studies are warranted to investigate the specific molecular mechanisms by which ITGB1 influences ITGA5 in regulating stemness in HCC cells. Furthermore, we observed the presence of ITGA5 in both the cell membrane and cytoplasm of HCC cells after they were treated with EVs. We speculate that it may be associated with the endocytosis of EVs by the recipient HCC cells. Integrins, which are transmembrane receptors found on the surface of cells or EV membranes, primarily undergo intracellular cycling through the process of endocytosis. Prior research has established that EVs can interact with target cells through various mechanisms, including endocytosis, direct binding, phagocytosis, and membrane fusion [43]. Consequently, if HCC cells endocytose EVs containing ITGA5, it would result in the appearance of ITGA5 within the cytoplasm of these cells.

CSCs are a subpopulation of tumor cells with strong self-renewal capabilities; they are key drivers of tumor progression, therapeutic resistance, disease recurrence, and metastasis [36, 44–46]. Recent studies have emphasized the close relationship between CSCs and resistance to immune checkpoint inhibitor (ICI) therapy in tumors. CSCs typically exhibit stronger immune evasion capabilities and can further influence the efficacy of ICIs by mediating the remodeling of the immune microenvironment [47]. ICI therapy is currently one of the most important treatment options for HCC. Nonetheless, it is limited by low efficacy and the development of resistance. Therefore, there is an urgent need to develop new methods for improving the response of HCC to ICIs. While evaluating the therapeutic effect of targeting ITGA5 in HCC, we also assessed the sensitization effect of ITGA5 inhibitors on ICI therapy for HCC. The results showed that ITGA5 inhibitors can inhibit the growth of orthotopic HCC in mice, reduce the proportion of infiltrating myofibroblasts and CSCs in the tumor, and significantly enhance the therapeutic effect of anti-PD-L1 antibodies when used in combination. These results indicate that ITGA5 is a potential therapeutic target for HCC and that targeting ITGA5 could represent a potential strategy for sensitizing HCC to ICI therapy.

Conclusions

In conclusion, our study demonstrated that ITGA5 is primarily expressed in myofibroblasts within HCC tissue, and high levels of ITGA5^{+} myofibroblasts are associated with poor prognosis in patients with HCC. Additionally, we identified a novel regulatory pathway in which myofibroblasts enhance the stemness of HCC cells by producing EVs that transfer ITGA5 to HCC

cells. Mechanistically, we found that ITGA5 primarily enhances HCC cell stemness by activating YES1 and its downstream pathways. Moreover, our study revealed that ITGA5 is a potential therapeutic target for HCC, and targeting ITGA5 represents a new strategy to improve the efficacy of immune therapy.

Materials and methods

Clinical samples

HCC specimens were obtained from 25 consecutive patients who had undergone curative liver resection at the Hepatobiliary Department of the First Affiliated Hospital of Jinan University (Guangzhou, China). The 19 normal hepatic tissues used as normal controls were obtained from patients with benign hepatic lesions who underwent resection in the Hepatobiliary Department of the First Affiliated Hospital of Jinan University. HCC samples with TMA of 84 patients, including survival data, were purchased from OUTDO Biotech (Shanghai, China).

Cell lines and cell culture

Human HCC cell line PLC/PRF/5, human HSC line LX-2, and murine HCC cell line Hep1–6 were obtained from the Shanghai Cell Bank of Chinese Academy of Science (Shanghai, China). Human HCC cell line Huh7 was a generous gift from Sun Yat-Sen University Cancer Center (Guangzhou, China). All cells were verified by short tandem repeat (STR) analysis. All these cells were cultured in high-glucose Dulbecco's modified Eagle's medium (DMEM) supplemented with 10% fetal bovine serum (FBS; ExCell, Suzhou, China) and 1% penicillin and streptomycin (ThermoFisher Scientific, Waltham, MA, USA). Primary human myofibroblasts were isolated from tumor specimens of patients with HCC who underwent liver resection in the First Affiliated Hospital of Jinan University. The isolation of myofibroblasts was performed as previously reported. The cells were cultured in DMEM/F12 supplemented with 10% FBS and 1% penicillin and streptomycin.

Animal models

4- to 6-week-old male BALB/c nude mice and C57BL/6 mice were purchased from Zhejiang Vital River Laboratory Animal Technology Co. Ltd (Zhejiang, China). The mice were bred in a specific pathogen-free environment with a 12-h cycle at a temperature of 22℃–25℃. Animal studies were approved by the Animal Care and Use Committee at Jinan University. The detailed procedure is described in the Supporting Materials and Methods.

Statistical analysis

Survival curves were generated via the Kaplan–Meier method. Categorical data were analyzed, and comparisons of continuous variables were performed with the chi-squared/Fisher's exact test and Student's *t*-test/Mann–Whitney *U* test, respectively. The data are represented as the mean ± standard deviations of at least three sample replicates. *P*-values < 0.05 indicate statistically significant differences. All analyses were performed with SPSS version 26.0 (IBM Corp., Armonk, NY, USA) and GraphPad Prism 8.4.3 (GraphPad Software Inc., San Diego, CA, USA).

Additional detailed materials and methods are described in the Supplementary Materials and Methods.

Abbreviations

ITGA5	Integrin α5
HCC	Hepatocellular carcinoma
EVs	Extracellular vesicles
TME	Tumor microenvironment
CSCs	Cancer stem cells
CAFs	Cancer associated fibroblasts
HSCs	Hepatic stellate cells
TCGA	The Cancer Genome Atlas
GEO	Gene Expression Omnibus
OS	Overall survival
DFS	Disease-free survival
MS	Mass spectrometry
Co-IP	Co-immunoprecipitation
IHC	Immunohistochemistry
IF	Immunofluorescence
TMA	Tissue microarray
α-SMA	α-Smooth muscle actin
Ctrl	Control
EPCAM	Epithelial cell adhesion molecule
GO	Gene Ontology
GSEA	Gene Set Enrichment Analysis
ITGA5-KO	ITGA5 knockout
CCl_4	Carbon tetrachloride
PD-L1	Programmed death-ligand 1

Supplementary Information

The online version contains supplementary material available at https://doi.org/10.1186/s12943-024-02170-0.

Supplementary Material 1: Figure S1. High ITGA5 expression was correlated with an unfavorable prognosis in patients with HCC. A. OS curves for HCC patients with high and low ITGA5 expression from TCGA and GEO (GSE14520) databases. B. Disease-free survival curves for HCC patients with high and low ITGA5 expression from TCGA and GEO (GSE14520) databases. Figure S2. ITGA5$^+$ myofibroblasts were enriched in fibrotic liver and HCC tissues. Representative immunofluorescence images of ITGA5 and α-SMA in human and mouse liver tissues with various types of lesions. Scale bars: 50 μm. Figure S3. ITGA5 was stably expressed in myofibroblasts or activated HSCs. A. Representative bright-field and IF co-staining images of ITGA5 and α-SMA in primary human myofibroblasts isolated from adjacent non-tumor and HCC tissues. Scale bar: 100 μm for bright-field images; 50 μm for IF images. B. Immunoblotting of ITGA5 and α-SMA in primary human myofibroblasts. C. Representative bright-field and IF co-staining Images of ITGA5 and α-SMA in primary mouse HSCs cultured for 1 or 7 days. D. Immunoblotting of ITGA5 and α-SMA in primary mouse HSCs cultured for 1 or 7 days. Figure S4. ITGA5 governed the proliferation and activation of myofibroblasts. A. Immunoblotting of ITGA5 protein levels in HCC cell lines and LX-2 cells. B. Immunoblotting of ITGA5 and α-SMA in

LX-2 cells with or without ITGA5 knockdown. C. CCK-8 assays of LX-2 cells with or without ITGA5 knockdown. D. RT-qPCR analysis of ITGA5 and HSC activation-related markers in LX-2 cells with or without ITGA5 knockdown. *P< 0.05; **P < 0.01; ***P < 0.001. All data were obtained from three independent experiments per group. Figure S5. Accumulation of ITGA5$^+$ myofibroblasts was associated with an unfavorable prognosis in HCC patients with poor tumor differentiation. A. Representative immunofluorescence images of ITGA5 and α-SMA in tissues obtained from HCC patients with good or poor tumor differentiation. Scale bar: 20 μm. B. OS curve of HCC patients with good or poor tumor differentiation based on the infiltration of ITGA5$^+$ myofibroblasts. Figure S6. Myofibroblasts transfer ITGA5 to tumor cells via EVs. A. ITGA5 protein levels in LX-2 cells (Vector or ITGA5 OE). B. ITGA5 protein levels in Huh7 cells treated with or without EVs from LX-2 cells (Vector or Flag-ITGA5). Figure S7. Endogenous overexpression of ITGA5 enhanced the stemness of HCC cells. A. Sphere formation of Huh7 cells transfected with ITGA5 overexpression plasmids and the vector control. Scale bar: 100 μm. B. Immunoblotting of ITGA5 and CSC markers in the indicated cells.***P< 0.001. All data were obtained from three independent experiments per group. Figure S8. Depletion of ITGA5 in myofibroblasts abolished the enhancement induced by myofibroblast-derived EVs on the proliferation of HCC cells. A. Colony formation assays of Huh7 cells cultured alone or co-cultured with CM from myofibroblasts (Ctrl, si-Ctrl, or si-ITGA5). B. Colony formation assay of Huh7 cells treated with or without EVs from myofibroblasts (Vector or ITGA5-KO). *P < 0.05; **P < 0.01; ***P< 0.001. All data were obtained from three independent experiments per group. Figure S9. Depletion of ITGA5 in myofibroblasts abolished the enhancement induced by myofibroblast-derived EVs on HCC aggressiveness. A. Migration and invasion assays of Huh7 cells cultured with or without CM from myofibroblasts (Ctrl, si-Ctrl, or si-ITGA5). B. Migration and invasion assays of Huh7 cells treated with or without EVs from myofibroblasts (vector or ITGA5-KO). C. Schematic of the lung metastasis mouse model. The mice were injected with HCC cells alone or co-injected with EVs derived from myofibroblasts (Vector or ITGA5-KO). D. Representative images of lungs and H&E staining of the indicated groups (n = 6 per group). *P < 0.05; **P < 0.01; ***P < 0.001. All data were obtained from three independent experiments per group. Figure S10. ITGA5 blockade alleviated the CSC-like property of HCC cells induced by myofibroblast-derived EVs. A. Structure of AV3 (ITGA5 inhibitor). B. IF staining showed a significant AV3-FAM/ITGA5 binding in HCC cells treated with EVs from LX-2 cells. Scale bar: 25 μm. C. Colony formation of HCC cells subjected to the indicated treatment. D. Sphere formation assays of the indicated groups. E. Immunoblotting of CSC markers in Huh7 or PLC/PRF/5 cells subjected to the indicated treatments. *P < 0.05; **P < 0.01; ***P < 0.001. All data were obtained from three independent experiments per group. Figure S11. ITGA5 expression was associated with immune cell infiltration and ICI-related gene expression in HCC. A. Correlation between ITGA5 expression and immune cell infiltration. B. Correlation between ITGA5 and immune checkpoint-related gene expression. C. Stroma scores of the HCC tissue in the high and low ITGA5 expression groups. *P < 0.05; **P< 0.01; ***P < 0.001. Data were obtained from the TCGA database. Figure S12. ITGA5-targeting therapy decreased MDSCs in HCC tissue. Representative images of dual immunofluorescence staining for CD11b (green) and Gr1 (red) in orthotopic HCC tissues extracted from the indicated groups. Scale bar: 50 μm. *P < 0.05; **P < 0.01; ***P < 0.001. Figure S13. ITGA5 blockade altered the immune microenvironment of orthotopic HCC tissues. A, B. PD-L1, CD11b, CD206, CD4, and CD8 expression in orthotopic HCC tissues from the indicated groups were detected by IHC staining (n = 4 for each group). Scale bar, 50 μm. *, P < 0.05; **, P< 0.01; ***P < 0.001. Figure S14. Inhibition of ITGA5 did not significantly affect the infiltration of M1 macrophages in the HCC mouse model. Representative IHC of CD86 in HCC tissues extracted from the indicated groups. Scale bar: 50 μm. Figure S15. ITGB1 participated in ITGA5-induced stemness of HCC cells. A. Immunoblotting of Huh7 cells with indicated treatment. B. Sphere formation of Huh7 cells with indicated treatment. *, P < 0.05; **, P < 0.01.

Supplementary Material 2.

Supplementary Material 3.

Acknowledgements
The authors would like to acknowledge the Medical Experimental center, School of Medicine, Jinan University and the Institute of Molecular and Medical Virology, Jinan University for providing us with necessary experimental support by supplying laser scanning confocal microscope, ultracentrifuge and other equipment for this study.

Authors' contributions
Y.X.: wrote the main manuscript text, designed the study, and performed in vitro and in vivo experiments. P.T.: reviewed the manuscript. KK.Z.: data analysis. LYC: performed in experiments. JY.L., HL.J. & L.H.: performed in experiments. ZW.C. & MR.C.: Sample collection. J.S. & J.H.: writing review. C.Q.: writing review, designed the study.

Funding
This work was supported by National Natural Science Foundation of China (Grant No. 82273154) and Guangdong Basic and Applied Basic Research Foundation (Grant No. 2023A1515012541).

Data availability
No datasets were generated or analysed during the current study.

Declarations

Ethics approval and consent to participate
The study was performed in accordance with the declaration of Helsinki. Human HCC samples were obtained from the First Affiliated Hospital of Jinan University under protocols approved by the Ethics Committee. Written informed consent was obtained from each patient. Animal experiment protocols were approved by the Institutional Animal Ethical Committee of the Experimental Animal Center of Jinan University.

Competing interests
The authors declare no competing interests.

Author details
[1]Department of Pathophysiology, School of Medicine, Jinan University, Guangzhou 510000, China. [2]Endoscopy Department, Sichuan Cancer Center, Sichuan Cancer Hospital and Institute, Affiliate Cancer Hospital of University of Electronic Science and Technology of China (UESTC), Chengdu 610000, China. [3]Department of Hepatobiliary Surgery, The First Affiliated Hospital of Jinan University, Guangzhou 510000, China. [4]Department of Radiotherapy, Affiliated Cancer Hospital and Institute of Guangzhou Medical University, Guangzhou 510000, China. [5]Department of Medical Biochemistry and Molecular Biology, School of Medicine, Jinan University, Guangzhou 510000, China.

Received: 28 July 2024 Accepted: 5 November 2024
Published online: 21 November 2024

References

1. Galle PR, Forner A, Llovet JM, et al. EASL clinical practice guidelines: management of hepatocellular carcinoma. J Hepatol. 2018;69(1):182–236.
2. Huang HY, Tsui YM, Ng IOL. Fueling HCC dynamics: interplay between tumor microenvironment and tumor initiating cells. Cell Mol Gastroenter. 2023;15(5):1105–16.
3. Chen Y, Kim J, Yang S, et al. Type I collagen deletion in αSMA+ myofibroblasts augments immune suppression and accelerates progression of pancreatic cancer. Cancer Cell. 2021;39(4):548-565.e6.
4. Filliol A, Saito Y, Nair A, et al. Opposing roles of hepatic stellate cell subpopulations in hepatocarcinogenesis. Nature. 2022;610(7931):356–65.
5. Kisseleva T, Cong M, Paik Y, et al. Myofibroblasts revert to an inactive phenotype during regression of liver fibrosis. P Natl Acad Sci USA. 2012;109(24):9448–53.
6. Yavuz BG, Pestana RC, Abugabal YI, et al. Origin and role of hepatic myofibroblasts in hepatocellular carcinoma. Oncotarget. 2020;11(13):1186–201.
7. Kisseleva T, Brenner D. Molecular and cellular mechanisms of liver fibrosis and its regression. Nat Rev Gastroenterol Hepatol. 2020;18(3):151–66.

8. Loh J-J, Li T-W, Zhou L, et al. FSTL1 secreted by activated fibroblasts promotes hepatocellular carcinoma metastasis and stemness. Can Res. 2021;81(22):5692–705.
9. Chen QT, Zhang ZY, Huang QL, et al. HK1 from hepatic stellate cell-derived extracellular vesicles promotes progression of hepatocellular carcinoma. Nat Metab. 2022;4(10):1306–21.
10. Thinn AMM, Wang Z, Zhu J. The membrane-distal regions of integrin α cytoplasmic domains contribute differently to integrin inside-out activation. Sci Rep. 2018;8(1):5067.
11. Hou J, Yan D, Liu Y, Huang P, Cui H. The roles of integrin α5β1 in human cancer. Onco Targets Ther. 2020;13:13329–44.
12. Zhang XY, Chen FY, Huang PR, et al. Exosome-depleted MiR-148a-3p derived from hepatic stellate cells promotes tumor progression via ITGA5/PI3K/Akt axis in hepatocellular carcinoma. Int J Biol Sci. 2022;18(6):2249–60.
13. Chen J, Ji T, Wu D, et al. Human mesenchymal stem cells promote tumor growth via MAPK pathway and metastasis by epithelial mesenchymal transition and integrin α5 in hepatocellular carcinoma. Cell Death Dis. 2019;6(10):425.
14. Shi Y, Shang J, Li Y, et al. ITGA5 and ITGB1 contribute to Sorafenib resistance by promoting vasculogenic mimicry formation in hepatocellular carcinoma. Cancer Med-Us. 2023;12(3):3786–96.
15. Wang JF, Chen YY, Zhang SW, et al. ITGA5 promotes tumor progression through the activation of the FAK/AKT signaling pathway in human gastric cancer. Oxid Med Cell Longev. 2022;2022((1942–0994 (Electronic))):8611306.
16. Li XY, Li L, Wu JY. The members of the miR-148/152 family inhibit cancer stem cell-like properties in gastric cancer via negative regulation of ITGA5. J Transl Med. 2023;21(1):105.
17. Zhou CC, Shen YM, Wei ZY, et al. ITGA5 is an independent prognostic biomarker and potential therapeutic target for laryngeal squamous cell carcinoma. J Clin Lab Anal. 2022;36(2):e24228.
18. Zheng WQ, Jiang CH, Li RF. Integrin and gene network analysis reveals that ITGA5 and ITGB1 are prognostic in non-small-cell lung cancer. Onco Targets Ther. 2016;9:2317–27.
19. Parola M, Pinzani M. Liver fibrosis: Pathophysiology, pathogenetic targets and clinical issues. Mol Aspects Med. 2019;65:37–55.
20. Song M, He J, Pan QZ, et al. Cancer-associated fibroblast-mediated cellular crosstalk supports hepatocellular carcinoma progression. Hepatology. 2021;73(5):1717–35.
21. Guo Q, Furuta K, Lucien F, et al. Integrin b1-enriched extracellular vesicles mediate monocyte adhesion and promote liver inflammation in murine NASH. J Hepatol. 2019;71:1193–205.
22. Mao L, Yuan W, Cai K, et al. EphA2-YES1-ANXA2 pathway promotes gastric cancer progression and metastasis. Oncogene. 2021;20(40):3610–23.
23. Hayashi HHT, Yokoyama N, Kaida T, Sakamoto K, Fukushima Y, Ishimoto T, Kuroki H, Nitta H, Hashimoto D, Chikamoto A, Oki E, Beppu T, Baba H. An imbalance in TAZ and YAP expression in hepatocellular carcinoma confers cancer stem cell–like behaviors contributing to disease progression. Can Res. 2015;22(75):4985–97.
24. Zhao D, Yin Z, Soellner MB, Martin BR. Scribble sub-cellular localization modulates recruitment of YES1 to regulate YAP1 phosphorylation. Cell Chem Biol. 2021;28(8):1235-1241.e5.
25. Garmendia I, Redin E, Montuenga LM, Calvo A. YES1: a novel therapeutic target and biomarker in cancer. Mol Cancer Ther. 2022;21(9):1371–80.
26. Jiang Y, Chen P, Hu K, et al. Inflammatory microenvironment of fibrotic liver promotes hepatocellular carcinoma growth, metastasis and sorafenib resistance through STAT3 activation. J Cell Mol Med. 2021;25(3):1568–82.
27. Davidson G, Helleux A, Vano YA, et al. Mesenchymal-like tumor cells and myofibroblastic cancer-associated fibroblasts are associated with progression and immunotherapy response of clear cell renal cell carcinoma. Cancer Res. 2023;83(17):2952–69.
28. Mhaidly R, Mechta-Grigoriou F. Fibroblast heterogeneity in tumor microenvironment: role in immunosuppression and new therapies. Semin Immunol. 2020;48:101417.
29. Qu C, He L, Yao N, et al. Myofibroblast-specific knockout inhibits HCC progression in a mouse model. Hepatology. 2021;74(1):458–73.
30. Kuninty PAO, Bansal RAO, De Geus SWL, et al. ITGA5 inhibition in pancreatic stellate cells attenuates desmoplasia and potentiates efficacy of chemotherapy in pancreatic cancer. Sci Adv. 2019;9(5):eaax2770.
31. Campbell ID, Humphries MJ. Integrin structure, activation, and interactions. Cold Spring Harb Perspect Biol. 2011;3(3): a00494.
32. Li S, Sampson C, Liu C, Piao HL, Liu HX. Integrin signaling in cancer: bidirectional mechanisms and therapeutic opportunities. Cell Commun Signal. 2023;1(21):266.
33. Chen JR, Zhao JT, Xie ZZ. Integrin-mediated cancer progression as a specific target in clinical therapy. Biomed Pharmacother. 2022;155: 113745.
34. Horn V, Cancino CA, Steinheuer LM, et al. Multimodal profiling of peripheral blood identifies proliferating circulating effector CD4(+) T cells as predictors for response to integrin α4β7-blocking therapy in inflammatory bowel disease. Gastroenterology. 2024;24(27): 005527.
35. Zhang C, Zhou T, Chen Z, et al. Coupling of integrin α5 to annexin A2 by flow drives endothelial activation. Circ Res. 2020;8(127):1074–90.
36. Tey SK, Wong SWK, Chan JYT, et al. Patient pIgR-enriched extracellular vesicles drive cancer stemness, tumorigenesis and metastasis in hepatocellular carcinoma. J Hepatol. 2022;76(4):883–95.
37. Fang JH, Zhang ZJ, Shang LR, et al. Hepatoma cell-secreted exosomal microRNA-103 increases vascular permeability and promotes metastasis by targeting junction proteins. Hepatology. 2018;68(4):1459–75.
38. Lin Z, Li G, Jiang K, Li Z, Liu T. Cancer therapy resistance mediated by cancer-associated fibroblast-derived extracellular vesicles: biological mechanisms to clinical significance and implications. Mol Cancer. 2024;1(23):191.
39. Hamanaka N, Nakanishi Y, Mizuno T, et al. YES1 is a targetable oncogene in cancers harboring YES1 gene amplification. Can Res. 2019;79(22):5734–45.
40. Pang Y, Liu Z, Han H, et al. Peptide SMIM30 promotes HCC development by inducing SRC/YES1 membrane anchoring and MAPK pathway activation. J Hepatol. 2020;73(5):1155–69.
41. Kim C, Ye F, Ginsberg MH. Regulation of integrin activation. Annu Rev Cell Dev Biol. 2011;27:321–45.
42. Emery A, Dunning KR, Dinh DT, Akison LK, Robker RL, Russell DL. Dynamic regulation of semaphorin 7A and adhesion receptors in ovarian follicle remodeling and ovulation. Front Cell Dev Biol. 2023;11:1261038.
43. Kalluri RAOX, LeBleu VAO. The biology, function, and biomedical applications of exosomes. Science. 2020;6478(367):eaau6977.
44. Liang NAO, Yang T, Huang Q, et al. Mechanism of cancer stemness maintenance in human liver cancer. Cell Death Dis. 2022;4(13):394.
45. Primeaux M, Liu X, Gowrikumar S, et al. Claudin-1 interacts with EPHA2 to promote cancer stemness and chemoresistance in colorectal cancer. Cancer Lett. 2023;573: 216479.
46. Sadrkhanloo M, Entezari M, Orouei S, et al. STAT3-EMT axis in tumors: modulation of cancer metastasis, stemness and therapy response. Pharmacol Res. 2022;182: 106311.
47. Zhang Z, Wang ZX, Chen YX, et al. Integrated analysis of single-cell and bulk RNA sequencing data reveals a pan-cancer stemness signature predicting immunotherapy response. Genome Med. 2022;1(14):45.

Publisher's Note